

SU(2) lattice gauge theory and the convergence of the t expansion

G. J. Mathews, N. J. Snyderman, and S. D. Bloom

University of California, Lawrence Livermore National Laboratory, Livermore, California 94550

(Received 26 May 1987)

We have extended the t expansion of Horn and Weinstein to higher order for Hamiltonian SU(2) lattice gauge theory. We have calculated connected matrix elements up to $\langle H^{12} \rangle^c$ in the vacuum sector and $\langle H^{11} \rangle^c$ in the string sector. These data are then utilized to compute the 0^{++} glueball mass M , the string tension σ , and their ratio $R = M^2/\sigma$. We find evidence for the convergence of the t expansion in that the calculations are improved by including higher-order terms. R appears to approach a constant value ($M/\sigma^{1/2} \simeq 3.3$) at weak coupling, which is consistent with Euclidean lattice Monte Carlo results.

I. INTRODUCTION

Recently,¹⁻⁸ there has been renewed interest in the Hamiltonian formalism⁹ for computing hadron masses from lattice gauge theory. This is partly due to the enormous scale of the computer calculations required by Euclidean Monte Carlo methods. The Hamiltonian formalism reduces the computational problem to three dimensions and allows for the elimination of a considerable amount of redundant information due to translational degeneracy. Hamiltonian strong-coupling perturbation theory, while it has the advantages that it is systematic and analytic, has the disadvantage that a finite series which accurately describes strong-coupling behavior must be extrapolated to weak coupling in order to obtain continuum results. A new alternative to strong-coupling perturbation theory is the t expansion of Horn and Weinstein,¹ which is analogous to the high-temperature series expansion in statistical mechanics. While once again there is a series extrapolation problem, it is now in an external parameter t ; all coefficients in the series are exact functions of the gauge coupling. Coefficients in the series in t are matrix elements of connected powers of the Hamiltonian $\langle H^n \rangle^c$. The computation of these matrix elements reduces to manipulations on connected-graph sublattices.

In this work, we have calculated matrix elements for the SU(2) lattice gauge theory up to order $\langle H^{12} \rangle^c$ in the vacuum sector and up to $\langle H^{11} \rangle^c$ in the string sector. The convergence of the Padé-extrapolated t expansion is improved over the calculations of Ref. 2 where only contributions up to $\langle H^{10} \rangle^c$ and $\langle H^7 \rangle^c$ were available for the vacuum and string sectors, respectively. The t expansion for the ratio of the 0^{++} glueball mass to the square root of the string tension, $R^{1/2} = M/\sigma^{1/2}$, shows signs of converging to a constant for values of the coupling near $g^2 \sim 1$, within the scaling regime. We deduce a value of $M/\sigma^{1/2} \simeq 3.3 \pm 0.2$, where the error is estimated from the consistency of numerous Padé extrapolations. This value for the ratio agrees with Euclidean lattice Monte Carlo results.¹⁰

We also compare results of the D -Padé extrapolated t expansion for M and σ separately with Padé-improved

strong-coupling perturbation theory.³ The two series agree well from strong coupling down to g^2 of order 2. However, for the mass ratio R , the apparent convergence to a constant from the t expansion is not matched by perturbation theory.

II. THE t EXPANSION

The SU(2) lattice gauge theory in $3+1$ dimensions is described by a Hamiltonian⁹ which has the form

$$H = (g^2/2a)T + (2/g^2a)V, \quad (1)$$

where g is the coupling constant and a is the lattice spacing. T is the sum of electric flux operators with values $j(j+1)$, $j=0, \frac{1}{2}, 1, \dots$, on every link of the lattice, and V is the sum of magnetic flux operators on each of the N plaquettes of the lattice. V acts on a given plaquette by changing j to $j \pm \frac{1}{2}$ on each of the four links of the plaquette. This Hamiltonian is discussed further in the Appendix where we derive the general matrix elements of V with respect to arbitrary eigenfunctions of T .

The generating function for the expectation value of connected powers of H (with respect to an arbitrary state),

$$\frac{\langle H e^{-tH} \rangle}{\langle e^{-tH} \rangle} = \sum_{n=0}^{\infty} \frac{(-t)^n}{n!} \langle H^{n+1} \rangle^c, \quad (2)$$

suggests a natural approximation scheme. If $|0\rangle$ is an approximation to the true vacuum state, such as the strong-coupling vacuum (or some variational trial state), then since

$$\frac{\langle 0 | H e^{-tH} | 0 \rangle}{\langle 0 | e^{-tH} | 0 \rangle} = \left[\frac{\langle 0 | e^{-tH/2} | 0 \rangle}{\langle 0 | e^{-tH} | 0 \rangle^{1/2}} \right] \times H \left[\frac{e^{-tH/2} | 0 \rangle}{\langle 0 | e^{-tH} | 0 \rangle^{1/2}} \right] \quad (3)$$

as $t \rightarrow \infty$, the state

$$|\Omega_t\rangle = \frac{e^{-tH/2} | 0 \rangle}{\langle 0 | e^{-tH} | 0 \rangle^{1/2}} \quad (4)$$

converges to the true vacuum state. Similarly, the gen-

erating function, which equals $\langle \Omega_t | H | \Omega_t \rangle = E(t)$, converges to the true vacuum energy as $t \rightarrow \infty$. [$E(t)$ is directly proportional to the volume, Na^3 , and thus, so are the connected matrix elements.] Calculation of the connected matrix elements $\langle H^n \rangle^c$ in Eq. (2) to a given order n gives $E(t)$ accurately for small t , but arbitrary g . This is the t expansion. The large- t behavior must be guessed by Padé or similar extrapolation methods.

The t expansion is the analog of the high-temperature series in statistical mechanics where $\langle e^{-tH} \rangle \rightarrow \text{tr}(e^{-\beta H})$. The vacuum energy corresponds to the internal energy in statistical mechanics, $E(t) \rightarrow U(\beta) = -(\partial/\partial\beta) \times \ln\{\text{tr}[\exp(-\beta H)]\}$. The trace is taken with respect to any complete set of states; in the strong-coupling basis, the t expansion and high-temperature series agree for $t = \beta \rightarrow \infty$.

Our goal is to compute the series in Eq. (2) to sufficiently high order so that the large- t behavior of the generating function, and thus the vacuum energy, can be extracted. From the t expansion for the vacuum energy, the 0^{++} glueball mass will be obtained from $E(t)$, cf. Eq. (17) below. In a similar way, by choosing an initial state in Eq. (2) containing a string of $j = \frac{1}{2}$ electric flux, the string tension will be obtained.

III. COMPUTATION OF $\langle H^n \rangle^c$

From the t expansion, the computation of eigenstates of the lattice Hamiltonian is reduced to finding connected matrix elements of powers of the Hamiltonian. This computation can be accomplished in the following sequence of steps. First, the connected graphs which contribute to a given power of $\langle H^n \rangle^c$ need to be delineated. The open connected graphs containing up to 4 plaquettes, and closed graphs of up to 16 plaquettes, are listed in a seminal paper by Balian, Drouffe, and Itzykson.¹¹ There are 16 topologically distinct connected graphs containing up to 4 plaquettes. We have identified 54 topologically distinct graphs with 5 plaquettes and 247 graphs with 6 plaquettes. In addition to listing the distinct graphs (indexed by i), we must determine a geometrical factor G_i associated with each graph. This factor enumerates the number of distinct orientations of the graph (excluding translations) on the infinite lattice. The total connected matrix element will then be the sum over the contributions from all of these connected graphs times their geometrical weight:

$$\langle H^n \rangle^c = \sum_i G_i h_i^n, \quad (5)$$

where h_i^n is the connected matrix element computed on the lattice of the connected graph i . This decomposition is an enormous simplification since lattice configurations are then limited to only a few links (≤ 20 in the present calculation) which can contribute to a connected graph, rather than $\sim 10^3$ which might contribute on a small lattice.

Given the lattice pertaining to a particular connected graph i , the h_i^n are then determined from the total matrix elements $\langle H^n \rangle_i$ by first making use of the recursion relation^{1,2} for connected matrix elements:

$$\langle H^{n+1} \rangle_i^c = \langle H^{n+1} \rangle_i - \sum_{p=0}^{n-1} \binom{n}{p} \langle H^{p+1} \rangle_i^c \langle H^{n-p} \rangle_i. \quad (6)$$

Computing $\langle H^n \rangle_i^c$ on a connected-graph lattice includes terms corresponding to the Hamiltonian acting only on subgraphs of this lattice. The contributions from these subgraphs must be subtracted out. If each subgraph A of the graph i occurs $g_{i,A}$ times, then the net connected matrix element for this graph, h_i^n , is computed recursively:

$$h_i^n = \langle H^n \rangle_i^c - \sum_A g_{i,A} h_A^n. \quad (7)$$

For example,

$$h_{\square\square\square\square}^n = \langle H^n \rangle_{\square\square\square\square}^c - 2h_{\square\square\square}^n - 3h_{\square\square}^n - 4h_{\square}^n, \quad (8)$$

where the series begins with, $h_{\square}^n = \langle H^n \rangle_{\square}^c$.

To evaluate $\langle H^n \rangle$ for a connected graph we utilize a basis of strong-coupling eigenstates generated by successive operations of the plaquette creation operator V on the strong-coupling vacuum of a lattice corresponding to the graph under consideration. A Hamiltonian matrix is then constructed in this basis. The determination of $\langle H^n \rangle$ can then be achieved by successive multiplications of the Hamiltonian matrix acting on the start vector corresponding to the strong-coupling ground state. As an illustration, consider the simplest connected graph, the graph for a single plaquette. The basis of states for this lattice will be

$$(|0\rangle, |\square_{1/2}\rangle, |\square_1\rangle, |\square_{3/2}\rangle, \dots), \quad (9)$$

where the subscripts denote the angular-momentum-like quantum number indicating the color-electric flux excited along each link. For this graph, the Hamiltonian matrix takes on a particularly simple tridiagonal form:

$$\begin{pmatrix} 0 & x & & & & \\ x & 3 & x & & & \\ & x & 8 & x & & \\ & & x & 15 & & \\ & & & \ddots & & \end{pmatrix} \begin{pmatrix} 1 \\ 0 \\ 0 \\ 0 \\ \vdots \end{pmatrix} = \begin{pmatrix} 0 \\ x \\ 0 \\ 0 \\ \vdots \end{pmatrix}, \begin{pmatrix} x^2 \\ 3x \\ x^2 \\ 0 \\ \vdots \end{pmatrix}, \begin{pmatrix} 3x^2 \\ 2x^2 + 9x \\ 11x \\ x^3 \\ \vdots \end{pmatrix}, \dots \quad (10)$$

Equation (10) also illustrates the results of several matrix multiplications. $\langle H^n \rangle$ is simply given by the amplitude for the strong-coupling vacuum basis state after the n th multiplication of H . Similarly, $\langle H^{2n} \rangle$ can be obtained from the dot product of the n th vector with itself.

In the present calculation the size of the basis required to compute a given power of n is $\sim P^{n/2}$, where P is the number of plaquettes on the graph. The growth in the size of the basis as n becomes large is currently the limitation of this approach. For larger graphs, the number of basis states and the size of the Hamiltonian matrix can, however, be reduced by a proper accounting for the symmetries of the graph. In the present work we have not made use of this simplification, which can be significant for graphs with closed surfaces. We are in

the process of utilizing this feature to extend the calculation to yet higher orders. For the immediate future it appears that we should be able to compute the vacuum graphs up to at least $\langle H^{16} \rangle^c$ before computer limitations are prohibitive.

Having computed the h_i^n , it becomes apparent that there are remarkable cancellations of terms which could contribute to $\langle H^n \rangle^c$. Many of the graphs which could in principle contribute at a given order cancel until a much higher order. Figure 1 lists the graphs which were included in the vacuum computation of $\langle H^{12} \rangle^c$; the numbers with each graph give the order at which it contributes nonvanishing matrix elements, and its geometric factor G_i . Note that although we have only extended the highest order from $\langle H^{10} \rangle^c$ to $\langle H^{12} \rangle^c$, this introduces considerably more structure into possible vacuum fluctuations, i.e., the number of connected graphs increases by more than 50%.

Except for a theorem that $\langle V^n \rangle^c$ has nonzero contributions only on a single plaquette and closed surfaces, we cannot prove in general which graphs will contribute at a given order. There are, however, some general rules of thumb. For the open vacuum graphs, in addition to the two operations of V required for each plaquette, at least one operation of T is required for each plaquette which is part of an open surface. For example, the two-plaquette lattice does not contribute until $\langle H^6 \rangle^c$, corresponding to four operations of V to cover the lattice and

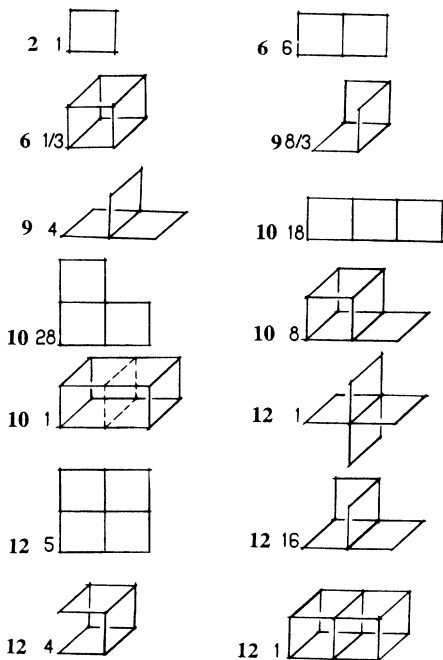


FIG. 1. Connected graphs that contribute to the calculation of $\langle H^{12} \rangle^c$ for the vacuum. The numbers before each graph specify the lowest order n of $\langle H^n \rangle^c$ at which they first give a nonzero contribution and the geometric factor G that counts the number of distinct ways the graph occurs on the lattice, excluding translation.

two operations of T . On closed-surface graphs, only one operation of V is required on each plaquette.

The connected matrix elements for the string tension can be obtained by repeating the calculation in the presence of a line of $j = \frac{1}{2}$ excited links in the initial and final states. Figure 2 shows the set of connected graphs that give nonzero contributions to the computation of the string tension up to $\langle H^{11} \rangle^c$. Note again that the number of connected graphs which contribute substantially increases when extending the calculation from $\langle H^7 \rangle^c$ to $\langle H^{11} \rangle^c$. The string graphs tend to give a nonvanishing contribution beginning at least one order higher than the corresponding vacuum graph. For example, two-plaquette graphs on a string begin to contribute at $\langle H^7 \rangle^c$.

For completeness we summarize here the connected matrix elements for the vacuum and string sectors. In

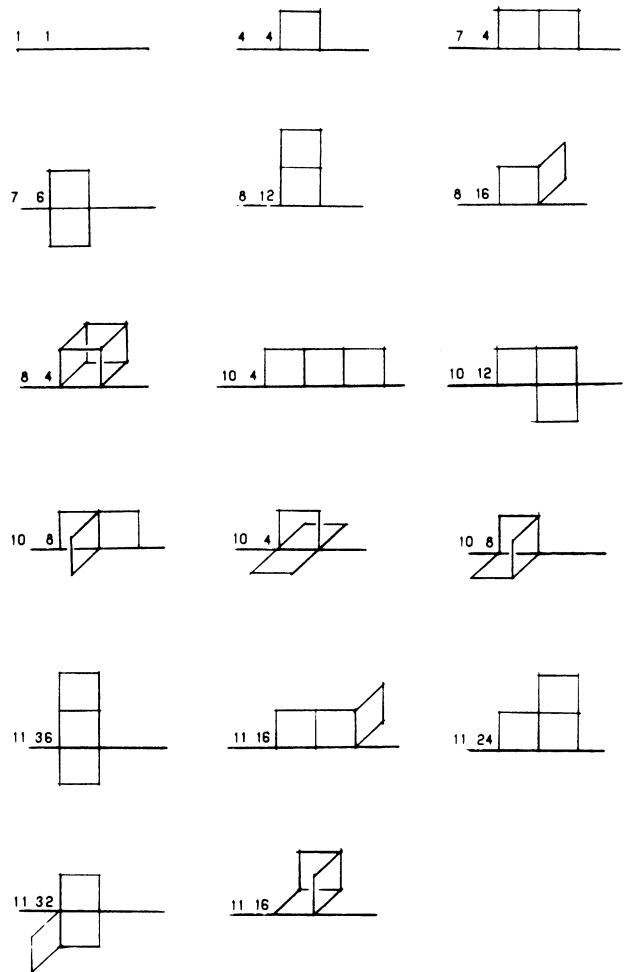


FIG. 2. Connected graphs which contribute to the calculation of the string tension to order $\langle H^{11} \rangle^c$. The numbers before each graph are n and G as defined in Fig. 1. Conspicuously absent are those three plaquette graphs that have only one plaquette edge in common with the string. These graphs are canceled to this order by the vacuum graphs.

the defining equations for connected powers of H , Eqs. (2) and (1), t and H are made dimensionless by the re-scaling, $tH = (g^2 t/a)[T + (4/g^4)V]$; if we now call $H = T + xV$, where $x = 4/g^4$, then the vacuum matrix elements are $g^2 N/2$ times

$$\begin{aligned}
\langle H^2 \rangle^c &= x^2, & \langle H^3 \rangle^c &= 3x^2, & \langle H^4 \rangle^c &= 9x^2 - x^4, \\
\langle H^5 \rangle^c &= 27x^2 - 10x^4, & \langle H^6 \rangle^c &= 81x^2 - 41x^4 + 20x^6, \\
\langle H^7 \rangle^c &= 243x^2 + 230x^4 + 420x^6, \\
\langle H^8 \rangle^c &= 729x^2 + 6740.5x^4 + 4942x^6 - 896x^8, \\
\langle H^9 \rangle^c &= 2187x^2 + 88889x^4 + 40331x^6 - 32256x^8, \\
\langle H^{10} \rangle^c &= 6561x^2 + 929120.125x^4 + 268951.125x^6 \\
&\quad - 635964x^8 + 65667x^{10}, \\
\langle H^{11} \rangle^c &= 19683x^2 + 8641747.625x^4 \\
&\quad + 3143657.5625x^6 - 8716686x^8 \\
&\quad + 3611685x^{10}, \\
\langle H^{12} \rangle^c &= 59049x^2 + 74960578.46875x^4 \\
&\quad + 82690581.625x^6 - 86932312.5x^8 \\
&\quad + 106624056x^{10} - 8036050x^{12}.
\end{aligned} \tag{11}$$

Our vacuum matrix elements agree with those computed up to $\langle H^{10} \rangle^c$ by Duncan and Roskies¹² using a different technique.

The net connected matrix elements in the string sector (after subtraction of the vacuum contribution) are $g^2 L/2$, where L is the number of links along the string, times

$$\begin{aligned}
\langle H^1 \rangle^c &= 0.75, & \langle H^4 \rangle^c &= 3x^2, & \langle H^5 \rangle^c &= 24x^2, \\
\langle H^6 \rangle^c &= 131.25x^2 - 15x^4, & \langle H^7 \rangle^c &= 611.25x^2 - 157.5x^4, \\
\langle H^8 \rangle^c &= 2610.1875x^2 + 1379.25x^4 + 840x^6, \\
\langle H^9 \rangle^c &= 10570.875x^2 + 65535.375x^4 \\
&\quad + 22396.5x^6, \\
\langle H^{10} \rangle^c &= 41337.890625x^2 + 1228949.25x^4 \\
&\quad + 293954.0625x^6 - 80640x^8, \\
\langle H^{11} \rangle^c &= 157753.359375x^2 + 17251026.5625x^4 \\
&\quad + 2432687.8125x^6 - 3519747x^8.
\end{aligned} \tag{12}$$

Our matrix elements for the string tension agree with Horn, Karliner, and Weinstein² up to the order that they calculated, $\langle H^7 \rangle^c$.

IV. APPLICATION

As was discussed in Ref. 2, the large- t behavior of the series can be extracted more reliably than by diagonal Padé extrapolation by constructing a rational function for the derivative of the series with respect to t , and then integrating over t (the so-called D -Padé method²).

An important quantity from which the Padé extrapo-

lations can be judged is the energy fluctuation

$$[\langle \Omega_t | H^2 | \Omega_t \rangle - (\langle \Omega_t | H | \Omega_t \rangle)^2] = -\frac{\partial E(t)}{\partial t}. \tag{13}$$

This quantity goes to a positive constant as $t \rightarrow 0$, and decreases monotonically to zero as $t \rightarrow \infty$ (since $|\Omega_t\rangle$ approaches an exact eigenstate of H). Therefore, $E(t)$ decreases monotonically with t to a constant value, for any value of g . Figure 3 shows an example of our results for $-\partial E/\partial t$ for the $[2/6]$ D -Padé extrapolation at different values of g^2 , and the unextrapolated finite series at $g^2=2$. The importance of the Padé extrapolation is evident from the breakdown of the finite series for $t \sim 0.5$, while the Padé extrapolation has the required behavior for much larger t . For $g^2=1.5$ the curve does not appear to approach zero asymptotically, indicative of a breakdown of the Padé extrapolation of the t series for small g^2 . For $g^2 \geq 2.0$, however, the Padé functions nicely reproduce the correct asymptotic behavior. Even though the integrand in the $[2/6]$ D -Padé function falls only as $1/t^4$ for large t , the convergence to asymptotic behavior occurs for t not much larger than 1, even for g^2 as small as 2. Once $-\partial E/\partial t$ gets very small, however, there are deviations from the correct asymptotic behavior; the curves either turn up after approaching zero, or overshoot and become negative. Since the asymptotic behavior is approached so rapidly in t , and then becomes unreliable, it is possible that in the calculations of $M(t)$ and $\sigma(t)$ the best asymptotic values for these quantities may actually be obtained at finite t . Thus, we also consider below Padé extrapolations for finite t .

A. 0^{++} glueball mass

The glueball mass is calculated² by use of the Lanczos algorithm to construct a zero-momentum state from

$$H | \Omega_t \rangle = \frac{e^{-tH/2} \sum_{\text{plaq}} | \square \rangle}{\langle 0 | e^{-tH} | 0 \rangle^{1/2}}, \tag{14}$$

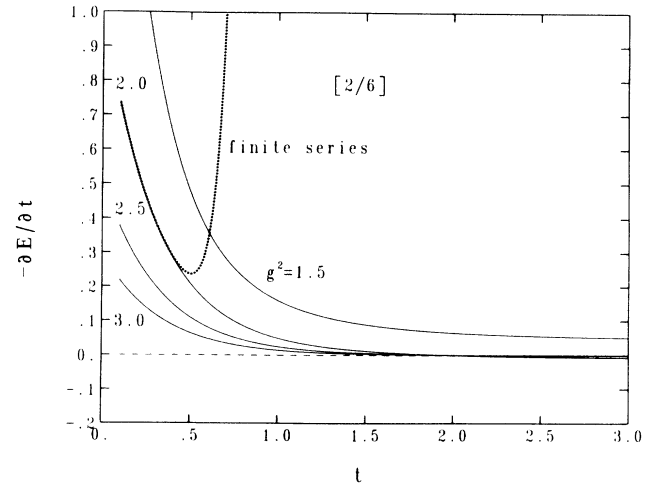


FIG. 3. $[2/6]$ D -Padé functions (solid lines) for $-\partial E/\partial t$ as a function of t for different values of g^2 . Also shown for comparison is the finite series for $\partial E/\partial t$ at $g^2=2$ (dotted line).

that is orthogonal to $|\Omega_t\rangle$. Such a normalized state is

$$|G_t\rangle = \frac{H|\Omega_t\rangle - |\Omega_t\rangle\langle\Omega_t|H|\Omega_t\rangle}{(\langle\Omega_t|H^2|\Omega_t\rangle - \langle\Omega_t|H|\Omega_t\rangle^2)^{1/2}}. \quad (15)$$

The 0^{++} glueball mass (mass gap) as a function of g^2 is then obtained from the $t \rightarrow \infty$ limit of

$$M(t, g^2) = \langle G_t | H | G_t \rangle - \langle \Omega_t | H | \Omega_t \rangle. \quad (16)$$

This formula can be conveniently reexpressed in terms of derivatives of $E(t)$:

$$M(t, g^2) = -\frac{g^2}{2a} \frac{\partial^2 E(t)/\partial t^2}{\partial E(t)/\partial t}. \quad (17)$$

After the differentiations of the series for $E(t)$, which is of order t^{11} , the resulting rational expression for $M(t, g^2)$ is reexpressed as a polynomial of order t^9 . Figure 4 shows the results from the [2/5] and [2/6] D -Padé approximations to $M(g^2)$; also shown, for reference, are the curves corresponding to the strong- and weak-coupling limits. The break away from strong coupling is for $g^2 \sim 5$, and the D -Padé extrapolations remain consistent until $g^2 \sim 2.2$. Although the match to weak-coupling scaling probably occurs for $g^2 \sim 2$, the slope at $g^2 \sim 2.2$ is already close to that of the weak-coupling curve.

Figure 5 shows $M(t, g^2)$ vs $2/g^2$, obtained by direct [2/4] and [3/5] Padé approximations to $M(t, g^2)$ for finite t chosen to best reproduce the weak-coupling behavior. Although the curve [3/5] in Fig. 5 seems to match nicely onto the weak-coupling scaling curve, it holds on to the strong-coupling behavior too long. From Figs. 4 and 5 it is apparent that there is better convergence to weak coupling when higher terms are included in the series.

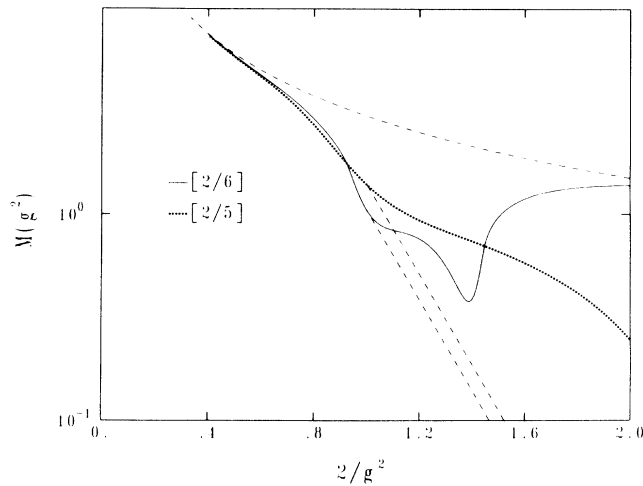


FIG. 4. D -Padé approximations to the series for the 0^{++} glueball mass, $M(g^2)$. The [2/6] (solid line) and [2/5] (dotted line) functions are compared to the strong- and weak-coupling limits (dashed lines). The two dashed weak-coupling lines are normalized to the Padé functions at $g^2=2$. They indicate the uncertainty in the determination of the glueball mass from these curves.

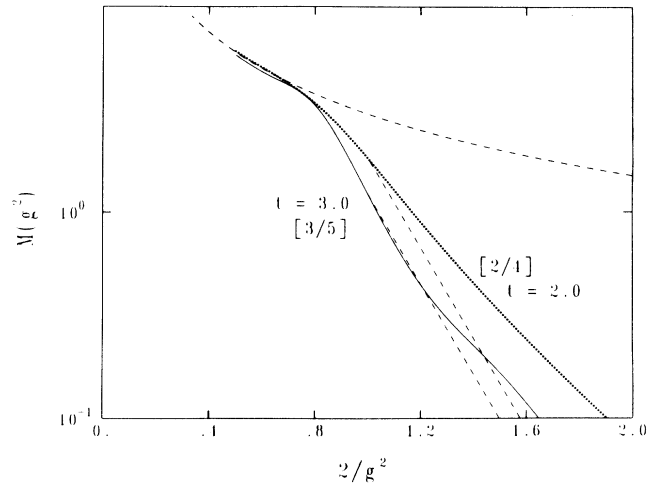


FIG. 5. Direct [2/4] and [3/5] Padé approximations to $M(g^2, t)$ for fixed values of t , which best extrapolate from strong to weak coupling.

Figure 6 shows various direct Padé extensions in $(4/g^4)^2$ for the strong-coupling perturbation series from Ref. 3. These curves show consistent behavior from strong coupling into the transition region. The agreement between the t -expansion D -Padé results (Fig. 4) and these curves is encouraging and suggests that the behavior of $M(g^2)$ is well defined at least into the transition region.

From the results of these extrapolations (Figs. 4 and 5) for M , we estimate that $M \sim (400 \pm 100)\Lambda$, where

$$\Lambda = (1/a)(12\pi^2/11g^2)^{51/121} \exp(-12\pi^2/11g^2). \quad (18)$$

The β function, which governs the way g must be rescaled with a , is extracted from the renormalization-group equation

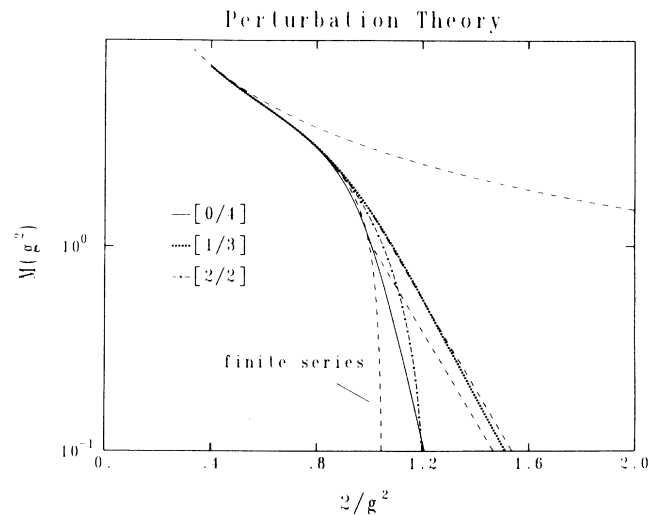


FIG. 6. Padé extensions of the strong-coupling perturbation series for $M(g^2)$ from Ref. 3.

$$\left[-a \frac{\partial}{\partial a} + \beta(g) \frac{\partial}{\partial g} \right] M(g, a) = 0. \tag{19}$$

The previous *D*-Padé determinations of *M* (Fig. 4) then determine the β functions shown in Fig. 7. They exhibit a consistent transition from strong coupling toward the asymptotic-freedom weak-coupling behavior.

B. String tension

Plotted in Figure 8 is the square root of the [2/5], [2/6], and [3/6] *D*-Padé extrapolations of the *t* series for the string tension. Although the string matrix elements were computed to almost as high an order as the vacuum matrix elements, they do not seem to contain nearly as much structure (compare Figs. 1 and 2). Perhaps, this is why the string-tension series are not as well defined as *M* when the weak-coupling regime is approached.

The results from the *D*-Padé series remain consistent from strong coupling to $g^2 \sim 2.2$. Although the curves do not yet match onto the weak-coupling scaling behavior, they suggest that scaling may possibly set in for $g^2 \sim 2$. It is unclear from this analysis whether the turn over to the weak-coupling slope is as rapid as the dip in the [2/5] and [3/6] *D*-Padé approximations or is much slower as indicated by the [2/6] *D*-Padé approximation.

Figure 9 shows direct Padé extensions of the series for σ for finite *t*. For these curves the transition away from the strong-coupling regime is not as consistently defined as for the *D*-Padé functions. Figure 10 shows the results of direct Padé extensions of the strong-coupling perturbation series in $(4/g^4)^2$ from Ref. 3. The results from the *D*-Padé extrapolations are consistent with strong-coupling perturbation theory into the transition region, although both methods are poorly defined at weak coupling.

From these curves we estimate that $\sigma^{1/2} \sim (200 \pm 100)\Lambda$.

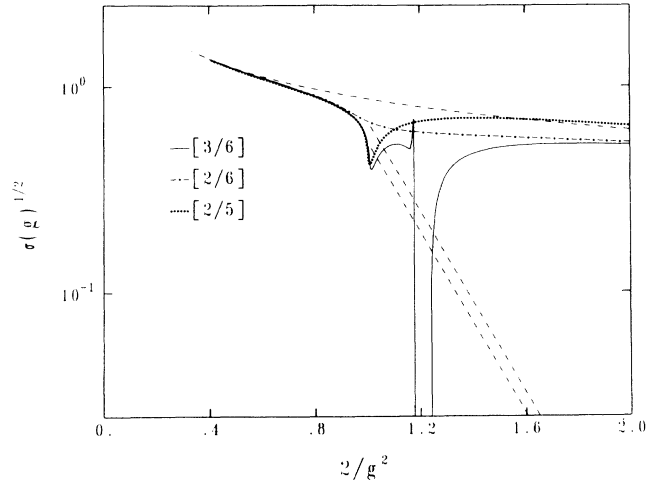


FIG. 8. Square root of the *D*-Padé approximations to the series for the string tension, $\sigma(g^2)$, for the [3/6] (solid line), [2/6] (dotted-dashed line), and [2/5] (dotted line) functions compared to the strong- and weak-coupling limits (dashed lines).

C. $R = M^2/\sigma$

From the calculations of *M* and σ separately, an estimate of $R^{1/2}$ can be obtained directly, $R^{1/2} \simeq 2 \pm 1$. However, a much more accurate determination can be made by first combining the series for the ratio of M^2 to σ , and retaining terms up to t^9 . The *D*-Padé extrapolations constructed from this series apparently have cancellations that allow extrapolation to much weaker coupling. Figure 11 shows the results for $R^{1/2}$ from the [0/5] to [0/8] and [1/4] to [1/7] *D*-Padé approximations. From this broad range of Padé extensions there is a trend toward a constant value of *R*, approached near $g^2 \sim 1$, before the calculations break down. The range of

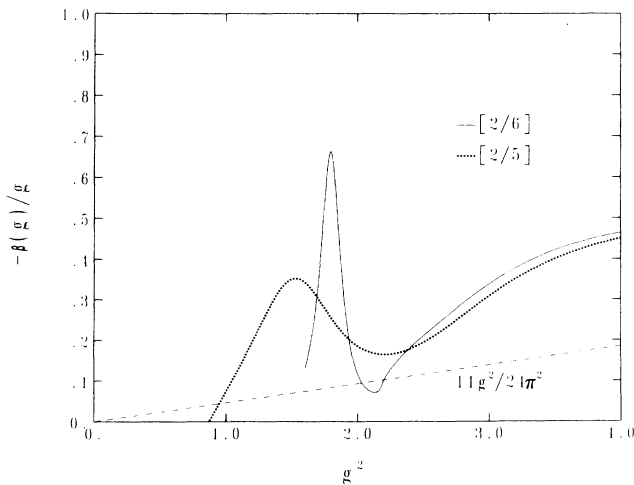


FIG. 7. β functions derived from the *D*-Padé approximations to *M*(g^2) of Fig. 4. The dashed curve shows asymptotic-freedom scaling.

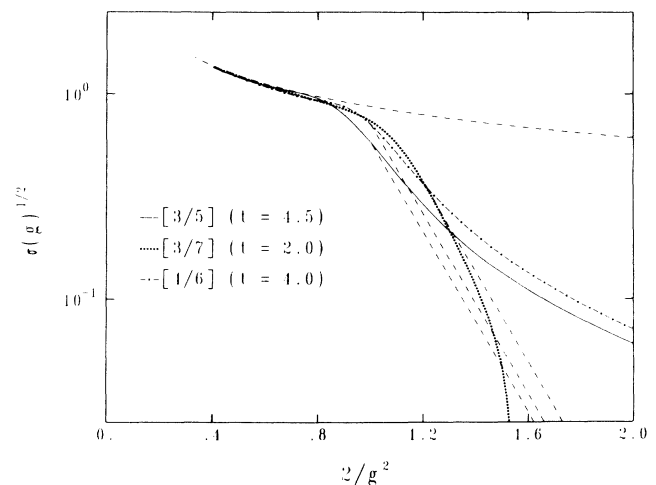


FIG. 9. Square root of the direct [3/5], [3/7], and [4/6] Padé approximations to $\sigma(g^2, t)$ for fixed values of *t* which best extrapolate from strong to weak coupling.

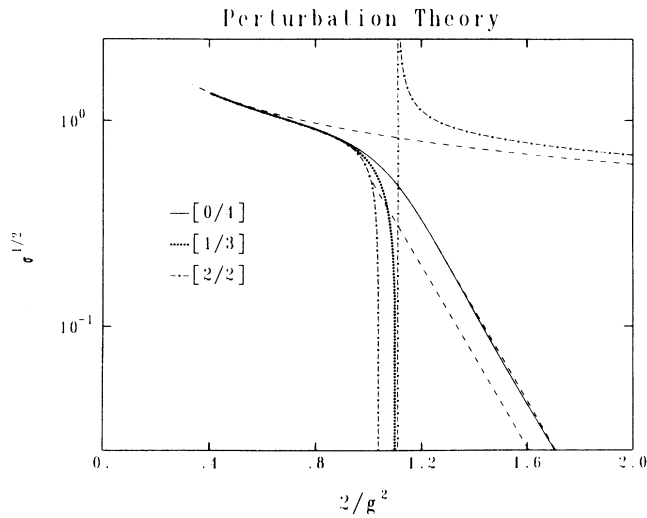


FIG. 10. Square root of various Padé extensions of the strong-coupling perturbation series for $\sigma(g^2)$ from Ref. 3.

g^2 for which $R^{1/2}$ approaches a constant is well below the peak in the Euclidean specific heat, which occurs for $g^2 \sim 2$, indicating the rapid cross over transition from strong-coupling to weak-coupling scaling behavior. The higher-order Padé curves exhibit a consistent convergence to a smaller value for R than the previous² lower-order (e.g., [0/5] and [1/4]) Padé evaluations. We deduce a value of $M/\sigma^{1/2} = 3.3 \pm 0.2$, which is within the quoted uncertainties² from lower-order calculations and is in good agreement with results from recent Euclidean lattice Monte Carlo calculations by DeGrand and Peterson¹⁰ who obtained a value of $M/\sigma^{1/2} = 3.4 \pm 0.3$.

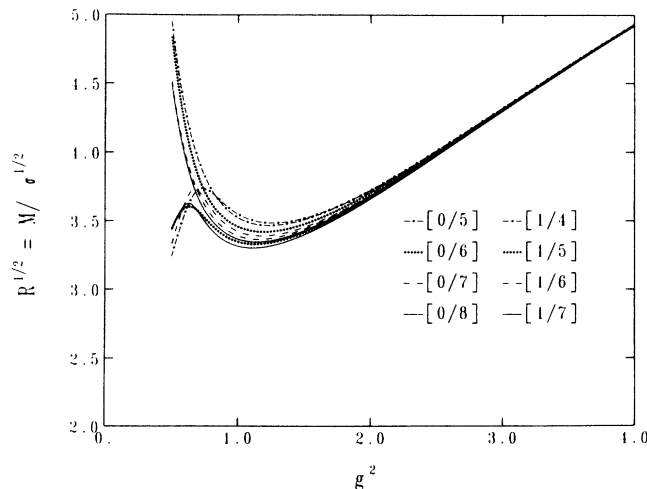


FIG. 11. Square root of various D -Padé approximations to the series for $R = M^2/\sigma$. The [0/ N] curves are the ones that decrease for $g^2 < 0.6$ and the [1/ N] curves are the ones that increase for $g^2 < 1.0$.

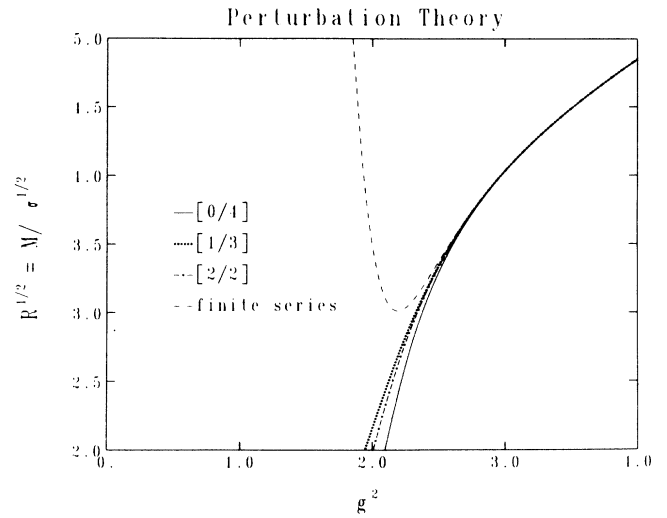


FIG. 12. Square root of various Padé extensions to the series for $R = M^2/\sigma$ derived from the strong-coupling perturbation series for M and σ from Ref. 3.

Figure 12, on the other hand, shows the results of different Padé extensions of the strong-coupling perturbation theory series for R constructed from the series for M and σ . These curves do not at all appear to have the correct behavior for small g^2 .

V. CONCLUSIONS

The weak-coupling behaviors of the glueball mass, the string tension, and their ratio are more clearly defined as the calculation is extended to higher order. The present results for $R^{1/2}$ also agree well with the value obtained from Euclidean lattice Monte Carlo calculations, although obtained with significantly less expenditure of computer time. (This entire calculation utilized approximately four hours of Cray XMP computer time.) At strong coupling, the t expansion accurately agrees with perturbation theory. For R , however, while perturbation theory does not converge to a constant at weak coupling, the t expansion does reasonably well. Nevertheless, given the need to extrapolate a series to large values of its expansion parameter, only convergence theorems and higher-order calculations will ultimately justify the method.

ACKNOWLEDGMENTS

The authors have benefited particularly from discussions with D. Horn, and also acknowledge useful discussions with T. Einwhoner, G. Guralnik, M. Karliner, A. Kerman, D. Levermore, S. Koonin, S. Libby, J. Louck, R. Roskies, D. Stump, and M. Zirnbauer. This work was performed under the auspices of the U.S. Department of Energy by Lawrence Livermore National Laboratory under Contract No. W-7405-ENG-48.

APPENDIX

In the Schrödinger formulation of the lattice quantum field theory for the gauge theory,⁹ the vector potential, $A = \mathbf{A} \cdot (\boldsymbol{\sigma}/2)$, and electric field $-E$ are canonically conjugate quantum variables (in $A^0=0$ gauge) on each link of a spatial lattice. The gauge-invariant magnetic field energy takes the form

$$a^3 \sum_{\text{plaq}} (1/g^2 a^4) [4 - \text{tr}(U_1 U_2 U_3^\dagger U_4^\dagger) - \text{tr}(U_4 U_3 U_2^\dagger U_1^\dagger)] = (2/g^2 a) V, \quad (\text{A1})$$

where $U = \exp[ig \mathbf{A} \cdot (\boldsymbol{\sigma}/2)a]$, and where the product in the traces is around the four links of a plaquette. [For SU(2) the two trace terms are equal.] This expression reduces to the Yang-Mills magnetic-field energy in the classical continuum limit. The rescaled color components of the vector potential, $g \mathbf{A} a = \boldsymbol{\theta}$, become angular variables; the SU(2) matrices, U , are then $j = \frac{1}{2}$ rotation matrices. The electric field operators, $\mathbf{E} = (g/a^2) i (\partial/\partial \boldsymbol{\theta})$, give for the electric field energy a Laplacian on S^3 , the SU(2) group manifold,

$$\frac{g^2}{2a} \sum_{\text{links}} -\nabla_{S^3}^2 = \frac{g^2}{2a} T. \quad (\text{A2})$$

The Hamiltonian

$$H = (g^2/2a)T + (2/g^2 a)V$$

then has the form of a nonrelativistic many-body (equal to the number of links of the lattice) Schrödinger operator with a four-body potential.

For strong coupling, there is a natural perturbation theory.¹³ The SU(2) rotation matrices form a complete set of eigenfunctions of the Laplacian on S^3 :

$$\begin{aligned} & \lim_{a \rightarrow 0} \left[E_x(\mathbf{n}) - [1 - ig A_x(\mathbf{n})a + \cdots] \left[E_x(\mathbf{n}) - a \frac{\partial E_x(\mathbf{n})}{\partial x} + \cdots \right] [1 + ig A_x(\mathbf{n})a + \cdots] \right] / a \\ & \rightarrow \frac{\partial E_x}{\partial x} + ig [A_x, E_x]. \end{aligned} \quad (\text{A5})$$

The commutator is only in the SU(2) Lie algebra, and is not canonical. Because of the correspondence $\mathbf{E} \rightarrow -(g/a^2)\mathbf{J}$, the second term in Eq. (A4) is $-g^2/a$ times an angular momentum operator in a rotated frame:

$$\frac{\boldsymbol{\sigma}}{2} \cdot \mathbf{J}' = -U^\dagger \frac{\boldsymbol{\sigma}}{2} U \cdot \mathbf{J}. \quad (\text{A6})$$

Referring to the labeling in Fig. 13 the states that respect the constraint of Gauss's law obey

$$(\mathbf{L}'_1 + \mathbf{L}_2 + \mathbf{S}'_1 + \mathbf{S}_2 + \mathbf{I}'_1 + \mathbf{I}_2) | \rangle = \mathbf{Q} | \rangle. \quad (\text{A7})$$

This requires the angular momenta on the links intersecting a given site to couple to zero (or to the angular momentum corresponding to a quark color state at the site). Defining basis states from the wave functions,

$$\langle U |^j_{mn} \rangle = (-1)^{j-m} \left(\frac{2j+1}{2\pi^2} \right)^{1/2} D^j_{-m,n}(U), \quad (\text{A8})$$

at each site of the lattice we adopt the coupling convention (see Fig. 13)

$$| \{ (l_1 l_2)_L (s_1 s_2)_S \} J (i_1 i_2)_I \}_{Q, \lambda} \rangle = \sum_{\{m\}} C_{n_1 m_2 M_L}^{l_1 l_2 L} C_{\nu_1 \mu_2 M_S}^{s_1 s_2 S} C_{M_L M_S M}^{LSJ} C_{\beta_1 \alpha_2 \kappa}^{i_1 i_2 I} C_{M \kappa \lambda}^{J I Q} \left| \begin{matrix} l_1 \\ m_1 n_1 \end{matrix} \right\rangle \left| \begin{matrix} l_2 \\ m_2 n_2 \end{matrix} \right\rangle \left| \begin{matrix} s_1 \\ \mu_1 \nu_1 \end{matrix} \right\rangle \left| \begin{matrix} s_2 \\ \mu_2 \nu_2 \end{matrix} \right\rangle \left| \begin{matrix} i_1 \\ \alpha_1 \beta_1 \end{matrix} \right\rangle \left| \begin{matrix} i_2 \\ \alpha_2 \beta_2 \end{matrix} \right\rangle. \quad (\text{A9})$$

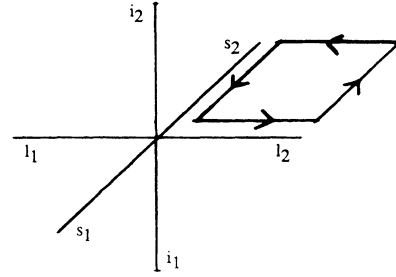


FIG. 13. Angular-momentum labels for links that intersect a given site. Also shown is a plaquette operator acting on the l_2 and s_2 links.

$$-\nabla_{S^3}^2 D^j_{mn}(U) = j(j+1) D^j_{mn}(U), \quad (\text{A3})$$

where, $j = 0, \frac{1}{2}, 1, \dots$, and the matrix elements of U (expressed in terms of Euler angles) parametrize the representation. The strong-coupling wave functions are products of rotation matrices of (in general) different j on each link, but subject to the constraint of Gauss's law.

The lattice covariant divergence of the color electric field is

$$\frac{E_x(\mathbf{n}) - U^\dagger E_x(\mathbf{n} - \hat{\mathbf{x}}) U}{a} \quad (\text{A4})$$

plus similar terms in y and z . Here \mathbf{n} refers to a lattice site, $E_x(\mathbf{n})$ is the color-electric field on the link in the $+x$ direction of \mathbf{n} , and U and $E_x(\mathbf{n} - \hat{\mathbf{x}})$ are the SU(2) rotation matrix and electric field Lie-algebra element on the link in the $-x$ direction of \mathbf{n} . In the naive continuum limit expression (A4) reduces to

These states satisfy the constraint of Eq. (A7), where the unprimed angular momentum operators act on the left magnetic quantum number,

$$J^z |^j_{mn} \rangle = m |^j_{mn} \rangle, \quad (\text{A10})$$

$$\begin{aligned} J^\pm |^j_{mn} \rangle &= \sum_{m'} [J^\pm(j)]_{m'm} |^j_{m'n} \rangle \\ &= [(j \mp m)(j \pm m + 1)]^{1/2} |^j_{m \pm 1, n} \rangle, \end{aligned}$$

and the primed operators act on the right magnetic quantum numbers in the same way. Gauss's law can be explicitly checked for these states using the standard recursion relation for Clebsch-Gordan coefficients derived from

$$\langle j_1 m_1 j_2 m_2 | J^\pm | j m \rangle = \langle j_1 m_1 j_2 m_2 | J_1^\pm + J_2^\pm | j m \rangle.$$

The general gauge-invariant state vector is then specified by not only the angular momentum on each link, but also the intermediate angular momenta at each site.

The action of V on a state changes j on each of the

four links of a plaquette by $\pm \frac{1}{2}$. The matrix elements of V are obtained from the wave functions corresponding to these states,

$$\int \Psi^*(U_1, U_2, \dots) V \Psi(U_1, U_2, \dots) dU_1 dU_2 \dots, \quad (\text{A11})$$

by integrating over the group manifold on all links. The integral on each link is evaluated using the familiar Clebsch-Gordan decomposition of representations and orthogonality of the rotation matrices:

$$\begin{aligned} \int D_{m'n'}^{j'*}(U) D_{\mu\nu}^{1/2}(U) D_{mn}^j(U) dU \\ = \frac{2\pi^2}{2j'+1} C_{\mu}^{1/2j} C_{m'm}^{j'} C_{\nu}^{1/2j} C_{n'n'}^{j'}. \end{aligned} \quad (\text{A12})$$

For each of the twelve orientations of a plaquette operator around a site, we recouple the standard angular momentum coupling convention of Eq. (A9) in order to naturally evaluate the part of the matrix element of V at that site. For example, for the plaquette operator in the orientation shown in Fig. 13, the recoupling¹⁴ is

$$\begin{aligned} | \{[(l_1 l_2)_L (s_1 s_2)_S]_J (i_1 i_2)_I\}_{Q,\lambda} \rangle &= \sum_{j_1 j_2} | \{[(l_1 s_1)_{j_1} (l_2 s_2)_{j_2}]_J (i_1 i_2)_I\}_{Q,\lambda} \rangle [(2j_1 + 1)(2j_2 + 1)(2L + 1)(2S + 1)]^{1/2} \\ &\times \begin{Bmatrix} l_1 & s_1 & j_1 \\ l_2 & s_2 & j_2 \\ L & S & J \end{Bmatrix}. \end{aligned} \quad (\text{A13})$$

In our present applications we will only need the expression for $Q=0, \lambda=0$ (no dynamical quarks). In terms of these recoupled states, the matrix element calculation simplifies since the part of the wave functions on all links not acted on by V are orthonormal. Then in this recoupled basis,

$$\begin{aligned} \langle \{[(l'_1 s'_1)_{j'_1} (l'_2 s'_2)_{j'_2}]_J (i'_1 i'_2)_{J'}\}_0 | \text{“}V\text{”} | \{[(l_1 s_1)_{j_1} (l_2 s_2)_{j_2}]_J (i_1 i_2)_J\}_0 \rangle \\ = \left[\frac{2l_2 + 1}{2s_2 + 1} \right]^{1/2} W(\frac{1}{2} l'_2 s_2 j_2; l_2 s'_2) \delta_{j_1 j'_1} \delta_{j_2 j'_2} \delta_{J J'} \delta_{l_1 l'_1} \delta_{s_1 s'_1} \delta_{i_1 i'_1} \delta_{i_2 i'_2}, \end{aligned} \quad (\text{A14})$$

where the quotation marks around V refer to only those terms in V that act on links that meet at the vertex in question. In this example, the relevant $D^{1/2}$ matrices are the first two terms of

$$\sum_{\text{plaq}} D_{\mu_1 \nu_1}^{1/2}(U_1) D_{\nu_1 \mu_2}^{1/2}(U_2) D_{\mu_2 \nu_2}^{1/2}(U_3^\dagger) D_{\nu_2 \mu_1}^{1/2}(U_4^\dagger), \quad (\text{A15})$$

where $D_{mn}^j(U^\dagger) = (-1)^{j-m} (-1)^{j-n} D_{-n, -m}^j(U)$. Also W is the standard Racah coefficient

$$W(\frac{1}{2} l'_2 s_2 j_2; l_2 s'_2) = (-1)^{(1/2) + l'_2 + s_2 + j_2} \begin{Bmatrix} \frac{1}{2} & l'_2 & l_2 \\ j_2 & s_2 & s'_2 \end{Bmatrix}. \quad (\text{A16})$$

Similar expressions are obtained for the other vertices associated with the plaquette operator acting in the plane, with the recoupling convention shown in Fig. 14. The arrows indicate the order of recoupling. For example, the recoupling order for vertex 2 is

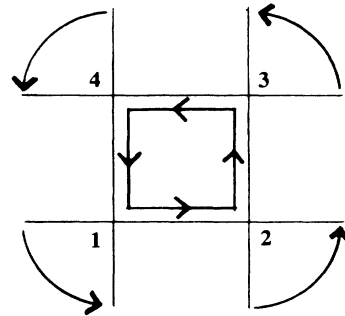


FIG. 14. Recoupling convention for a plaquette operator acting in the xy plane. At vertex 1 [cf. Eq. (A13)], $LS \rightarrow jj$ coupling. For vertex 2 the recoupling is described in Eq. (A17). Vertex 3 differs by a phase factor $(-1)^{j_1 + j_2 - J}$ relative to vertex 1 due to the interchange of j_1 and j_2 . Vertex 4 differs from vertex 2 by $(-1)^{K_1 + K_2 - J}$ due to the interchange of K_1 and K_2 .

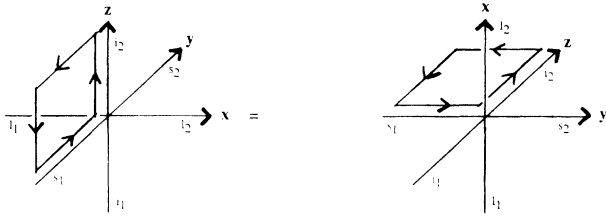


FIG. 15. Example of an out-of-plane plaquette considered as in plane due to a rotation of axes $(xy)z \rightarrow (yz)x$. Standard $(LS)I$ coupling is recoupled in this example to “standard” $(SI)L$ coupling. The matrix element is then calculated just as for a plaquette in the xy plane.

$$|[(l_1 l_2)_L (s_1 s_2)_S]_J\rangle \rightarrow |[(s_1 l_2)_{K_1} (s_2 l_1)_{K_2}]_J\rangle. \quad (\text{A17})$$

The general form of the matrix element is then a product of contributions associated with each vertex of the plaquette; the term at each vertex is a Racah coefficient times two $9-j$ recoupling coefficients: one from recoupling the initial state and one from the final state. There are also phase factors (zero in this example) and factors of $\sqrt{2j+1}$ from each matrix element and recoupling.

For plaquette operators out of the plane, the axes can be rotated so that the plaquette lies in the plane, as illustrated with an example in Fig. 15. After recoupling,

$$| \{ [(l_1 l_2)_L (s_1 s_2)_S]_J (i_1 i_2)_J \} \rangle \\ = | \{ [(s_1 s_2)_S (i_1 i_2)_J]_L (l_1 l_2)_L \} \rangle \quad (\text{A18})$$

(in this example the recoupling coefficient $\langle [(SJ)_L L]_0 | [(LS)_J J]_0 \rangle = 1$; other cases give phases),

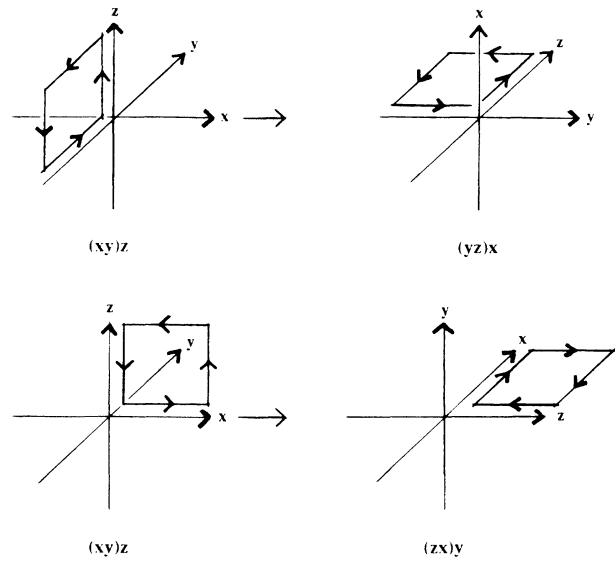


FIG. 16. Rotation of axes necessary for converting out-of-plane plaquettes to in-plane plaquettes.

the matrix element is obtained by transcription. As illustrated in Fig. 16, the axes must be rotated in cyclic order, since the original coupling scheme has a natural $(xy)z$ orientation. For the plaquette originally in the z - x plane, after rotation of the axes, the loop is oppositely oriented; the transcription of labels then requires that the vertices be identified in the order $1234 \rightarrow 2143$.

¹D. Horn and M. Weinstein, Phys. Rev. D **30**, 1256 (1985).

²D. Horn, M. Karliner, and M. Weinstein, Phys. Rev. D **31**, 2589 (1985).

³A. C. Irving, T. E. Preece, and C. J. Hamer, contributed paper to the XXIII International Conference on High Energy Physics, Berkeley, 1986 (unpublished).

⁴S. A. Chin, O. S. van Roosmalen, E. A. Umland, and S. E. Koonin, Phys. Rev. D **31**, 3201 (1985).

⁵C. P. Van Den Doel and D. Horn, Phys. Rev. D **33**, 3011 (1986).

⁶D. W. Heys and D. R. Stump, Phys. Rev. D **30**, 1315 (1984).

⁷A. Duncan and R. Roskies, Phys. Rev. D **31**, 364 (1985).

⁸G. J. Mathews, S. D. Bloom, and N. J. Snyderman, in *Proceedings of Intersections between Particle and Nuclear Physics*, edited by D. F. Geesamen (AIP Conf. Proc. No. 150) (AIP, New York, 1986), pp. 791–795.

⁹J. Kogut and L. Susskind, Phys. Rev. D **11**, 395 (1975).

¹⁰T. A. DeGrand and C. Peterson, Phys. Rev. D **34**, 3180 (1986); see also references cited in Ref. 2.

¹¹R. Balian, J. M. Drouffe, and C. Itzykson, Phys. Rev. D **11**, 2104 (1975).

¹²R. Roskies (private communication).

¹³The derivation of the matrix elements has also been independently performed by the following: D. Robson and D. M. Webber, Z. Phys. C **15**, 199 (1982); and J. Piekaremicz, M. R. Zirnbauer, and S. E. Koonin, J. Mod. Phys. A (to be published).

¹⁴See for example, L. C. Biedenharn and J. D. Louck, *Encyclopedia of Mathematics and Its Applications* (Addison-Wesley, Reading, Massachusetts, 1981), Vols. 8 and 9. Recoupling algebra is simplified by the use of coupling tree techniques described in Vol. 9.